Cryptospecies and crust effects on the geochemistry of Globorotalia inflata

Lukas Jonkers[1], Akshat Gopalakrishnan[2], Lea Weßel[2], Cristiano Mazur Chiessi[3], Jeroen Groeneveld[4], Patrick Monien[4], Douglas Lessa[5], and Raphael Morard[1]

[1]MARUM
[2]Department of Geosciences, University of Bremen
[3]University of São Paulo
[4]University of Bremen
[5]Universidade Federal Fluminense, Université Pierre et Marie Curie

November 22, 2022

Abstract

Sedimentary specimens of the planktonic foraminifera Globorotalia inflata can provide much needed information on subsurface conditions of past oceans. However, interpretation of its geochemical signal is complicated by possible effects of cryptic diversity and encrustation. Here we address these issues using plankton tow and sediment samples from the western South Atlantic, where the two genotypes of G. inflata meet at the Brazil-Malvinas Confluence Zone. The 18O and δ13C of encrusted specimens from both genotypes from a core within the confluence zone are indistinguishable. However, we do find a large influence of encrustation on δ18O and Mg/Ca. Whereas crust Mg/Ca ratios are at all locations lower than lamellar calcite, the crust effect on δ18O is less consistent in space. Plankton tows show that encrusted specimens occur at any depth and that even close to the surface crust Mg/Ca ratios are lower than in lamellar calcite. This is inconsistent with formation of the crust at lower temperature at greater depth. Instead we suggest that the difference between the crust and lamellar calcite Mg/Ca ratio is temperature-independent and due to the presence of high Mg/Ca bands only in the lamellar calcite. The variable crust effect on δ18O is more difficult to explain, but the higher incidence of crust free specimens in warmer waters and the observation that a crust effect is clearest in the confluence zone, hint at the possibility that the difference reflects advective mixing of specimens from warmer and colder areas, rather than vertical migration.

Cryptospecies and crust effects on the geochemistry of *Globorotalia inflata*

Lukas Jonkers1, Akshat Gopalakrishnan2, Lea Weßel2, Cristiano M. Chiessi3, Jeroen Groeneveld4, Patrick Monien2, Douglas Lessa5 and Raphael Morard1

1 MARUM center for Marine Environmental Sciences, University of Bremen, Leobener Straße 8, 28359 Bremen, Germany

2 Department of Geosciences, University of Bremen, Klagenfurter Str. 2-4, 28359 Bremen, Germany

3 School of Arts, Sciences and Humanities, University of São Paulo, Av. Arlindo Bettio 1000, 03828-000 São Paulo SP, Brazil

4 Alfred Wegener Institute, Helmholtz Center for Polar and Marine Research, Telegrafenberg A45, 14473 Potsdam, Germany

5 Programa de Pós-Graduação em Geoquímica, Federal Fluminense University, Outeiro São João Batista s/n, 24020-141 Niterói RJ, Brazil

ORCIDs:

Lukas Jonkers: 0000-0002-0253-2639

Jeroen Groeneveld: 0000-0002-8382-8019

Cristino M. Chiessi: 0000-0003-3318-8022

Patrick Monien: 0000-0002-4000-5362

Douglas Lessa: 0000-0002-2718-5901

Raphael Morard: 0000-0002-1181-5358

Key points

1. No direct genotype effect on stable isotope composition of *Globorotalia inflata*
2. Encrustation effect on geochemistry inconsistent with vertical migration
3. Differences between crust and lamellar calcite may reflect banding or advection

Abstract

Sedimentary specimens of the planktonic foraminifera *Globorotalia inflata* can provide much needed information on subsurface conditions of past oceans. However, interpretation of its geochemical signal is complicated by possible effects of cryptic diversity and encrustation. Here we address these issues using plankton tow and sediment samples from the western South Atlantic, where the two genotypes of *G. inflata* meet at the Brazil-Malvinas Confluence Zone. The $\delta^{18}O$ and $\delta^{13}C$ of encrusted specimens from both genotypes from a core within the confluence zone are indistinguishable. However, we do find a large influence of encrustation on $\delta^{18}O$ and Mg/Ca. Whereas crust Mg/Ca ratios are at all locations lower than lamellar calcite, the crust effect on $\delta^{18}O$ is less consistent in space. Plankton tows show that encrusted specimens occur at any depth and that even close to the surface crust Mg/Ca ratios are lower than in lamellar calcite. This is inconsistent with formation of the crust at lower temperature at greater depth. Instead we suggest that the difference between the crust and lamellar calcite Mg/Ca ratio is temperature-independent and due to the presence of high Mg/Ca bands only in the lamellar calcite. The variable crust effect on $\delta^{18}O$ is more difficult to explain, but the higher incidence of crust free specimens in warmer waters and the observation that a crust effect is clearest in the confluence zone, hint at the possibility that the difference reflects advective mixing of specimens from warmer and colder areas, rather than vertical migration.

Introduction

Globorotalia inflata is a subsurface dwelling planktonic foraminifera commonly encountered in subtropical to subpolar areas (Bé & Hutson, 1977; Lončarić et al., 2006; Niebler & Gersonde, 1998; Wilke et al., 2006). The chemical composition, in particular the stable oxygen isotope and Mg/Ca ratio, of its shell is often used to reconstruct subsurface ocean conditions (Groeneveld & Chiessi, 2011; Moffa-Sánchez et al., 2014; Santos et al., 2020). The morphospecies *G. inflata* contains two different genotypes, with type I associated with subtropical waters in both hemispheres and type II restricted to the subpolar waters of the southern hemisphere (Morard et al., 2011). These genotypes show subtle differences in shell morphology (Morard et al., 2016). However, the two types are not distinguished in palaeoceanographic studies despite different ecological preferences of the two genotypes, which may affect their seasonal or vertical habitat and hence their chemical composition (Morard et al., 2013) . It is also possible (or suspected) that biological differences between the genotypes of *G. inflata* may induce differences in biomineralisation and hence cause their geochemical proxy signals to differ, irrespective of their ecology. In other words, it is unknown if grown under the same conditions, genotype I and II would have the same or different chemical composition. There are indications from other species that genotypes may have different seasonal or vertical habitat preferences (Marshall et al., 2015) and for genotypical controls on shell composition (Sadekov et al., 2016). However, despite the obvious implications for palaeoceanographic reconstructions no studies exist that investigate the influence of cryptic diversity on the geochemistry of *G. inflata*.

Next to the unresolved issue of a possible effect of cryptic diversity on its geochemistry, *G. inflata* is also a species that forms a crust that often covers most of the lamellar calcite. In many species of foraminifera such crusts may account for a significant proportion of the shell mass and since crusts may have a markedly different composition from the lamellar calcite, crusting could affect the whole shell geochemistry (Bolton & Marr, 2013; Lohmann, 1995). Several studies have shown that sedimentary *G. inflata* have markedly higher $\delta^{18}O$ than those found in the water column and attributed this difference to encrustation at lower temperatures at greater depths (Lončarić et al., 2006; Mortyn & Charles, 2003). This pattern is consistent with the often lower Mg/Ca ratio of encrusted specimens (Groeneveld & Chiessi, 2011). Microanalytical techniques have also helped to reveal a clear Mg/Ca two-layer structure within the chamber walls of encrusted shells, with low Mg/Ca ratios in the crust and high ratios in the lamellar calcite (Hathorne et al., 2009; van Raden et al., 2011). Moreover, the Mg/Ca ratio of the lamellar calcite is in many species highly variable and

80   displays clear banding with a magnitude of several mmol/mol that is unrelated to temperature

         (Eggins et al., 2004; Jonkers et al., 2016; Spero et al., 2015). Such banding is also present in the

         lamellar calcite of *G. inflata* (Hathorne et al., 2009).

         The origin of the crust in *G. inflata* is unclear. In some, mostly spinose, species of foraminifera, crusts

85   may form in association with gametogenesis (Bé, 1980), whereas in others the origin is less clear and

         the crust consists of large euhedral crystals (Bé & Ericson, 1963; Hemleben et al., 1985). The

         composition of the crust suggests that it forms at lower temperatures, likely deeper in the water

         column and associated with ontogenetic downward migration (Bé & Ericson, 1963; Orr, 1967).

         However, crusts are also formed under isothermal conditions arguing against a temperature control

90   on crust formation (Davis et al., 2017; Jonkers et al., 2016). Culture studies using *G. inflata* have

         shown that it may form a crust at high temperatures (18–20 °C) shortly after gametogenesis

         (Hemleben et al., 1985). These authors only describe the initial stages of crust formation, where only

         patches of a smooth layer are visible on the outside of the shell wall. However, when fully encrusted

         with a smooth outer surface, the cross sectioned shells reveal large, blocky crystals that are more

95   reminiscent of real, non-gametogenic, crusts (Hathorne et al., 2009). Few, if any, direct observations

         from the water column exist to support the idea that encrustation in *G. inflata* (and perhaps in other

         species too) results from vertical downward migration. To the best of our knowledge, the single

         study explicitly investigating encrustation of *G. inflata* in the water column (Rebotim et al., 2019),

         showed that encrusted specimens are not restricted to the subsurface. This would argue against

100   vertical migration and temperature as a thermal trigger for crust formation. The different

         composition of the crust may hence also be due to different calcification mechanisms in crust and

         lamellar calcite (Bolton & Marr, 2013).

         Given the potentially large effects of both genotype variability and encrustation on the

105   environmental signal contained in the composition *G. inflata* it is important to i) determine if the

         genotypical variability leaves an imprint on its geochemistry; and ii) better constrain the effects and

         origin of the crust. Here we use plankton tow and sediment samples from the western South

         Atlantic, where the two genotypes meet at the highly dynamic Brazil-Malvinas Confluence Zone. We

         make use of subtle, yet distinctive differences in shell morphology to distinguish between type I and

110   II and assess the influence of genotypical variability on the stable oxygen and carbon isotope ratios

         of *G. inflata* in a sediment core from within the Brazil-Malvinas Confluence Zone (BMCZ). In addition,

         we assess the effect of crusting on $\delta^{18}O$ and $\delta^{13}C$ as well as Mg/Ca on water column and core top

         sediment samples from a north to south transect that crosses the BMCZ. Our analyses reveal no

direct cryptospecies effect, but highlight surprising differences in the effect of crusting on $\delta^{18}O$, $\delta^{13}C$

115   and Mg/Ca ratios. We present a hypothesis that explains this paradox.

Material and methods

Samples

We use samples from five sediment cores from a north-south transect that crosses the BMCZ (Fig. 1; Table I). We analysed down core samples in core GeoB13862-1 where both genotypes occur and

120   restricted analyses to the core tops (0-1 cm, dated as modern (Groeneveld & Chiessi, 2011)) in the remaining cores. In addition, we use samples from three stratified plankton nets (0-700 m) from the Malvinas Current and the BMCZ collected in January 2017 during Meteor cruise M133 (Fig. 1; Table II). The plankton net samples (>100 µm) were picked on board and preserved at -80 °C.

Classification of genotypes and encrustation

125   To test the influence of genotypical variability on the stable oxygen and carbon isotope ratio of *G. inflata*, specimens in the 300-1000 µm fraction from core GeoB13862-1 from the BMCZ were separated into the two genotypes. These two cryptic species of *G. inflata* have been shown to display subtle morphological differences in the relative size of the aperture (Morard et al., 2011) allowing a correct classification of 80% of specimens subjected to morphometric analyses (Morard et

130   al., 2016). Because precise morphometric analyses are time consuming, we performed a visual separation of *G. inflata* specimens into three categories. We considered specimens with large or small apertures relative to the size of the last camber to belong to genotype I or II respectively (Fig. 2). Specimens that could not be clearly attributed to either of these categories were classified as intermediate (Figure 2). Counts were performed on sample splits containing at least 300 planktonic

135   foraminifera shells and we restrict our geochemical analysis to specimens that could be clearly assigned to either type.

The crust effect on stable isotope ratios of *G. inflata* was assessed by measuring encrusted and non-encrusted specimens from all sediment cores separately. These groups were distinguished using

140   light microscopy. Specimens without encrustation are characterized by rougher or even spiky surfaces compared to encrusted specimens that display smooth, porcelaneous-looking, surfaces (Fig. 3). Since some specimens were previously picked from the core top samples without regard to encrustation, estimates of the relative proportions of encrusted and non-encrusted specimens may

be compromised. We note however that non-encrusted specimens are very rare and consider our
estimates to be, to a first order, correct.

Geochemical analyses

The influence of genotypical variation and encrustation on the stable oxygen and carbon isotope ratios of *G. inflata* were determined using conventional isotope ratio mass spectrometry. Before analysis, the samples were cleaned using repeated sonication with distilled water and ethanol. Measurements were performed on groups of 3 shells in the 300–1000 µm fraction in core GeoB13862-1 and on groups of 3–10 shells in the 150–1000 fraction in the core top samples using a Thermo MAT 253plus coupled to a Kiel IV device at MARUM (we rule out a possible size effect on our interpretations in the supplementary information). Analytical precision was determined through repeat measurements of an in-house carbonate standard (Solnhofen limestone), which was calibrated to the NBS 19 calcite standard, and amounted to 0.06 and 0.03 ‰ for $\delta^{18}O$ and $\delta^{13}C$, respectively.

The crust effect on the Mg/Ca ratios was investigated using laser ablation inductively coupled mass spectrometry (LA-ICP-MS), which renders it possible to determine element/calcium ratios in cross sections through the shell walls and therefore does not require separate measurements on encrusted and crust-free shells. Prior to laser ablation analysis specimens from sediment samples (300–425 µm) were cleaned using multiple sonication steps with distilled water and ethanol. No further cleaning was performed as areas of suspected contamination in the element/calcium profiles were excluded from analysis (see below). Specimens from plankton tow samples (>100 µm) were treated to remove organic matter. A 10-minute oxidizing step at 98 °C was applied twice with a 1%-H_2O_2 solution buffered with 0.1 M NaOH. To remove any oxidizing reagent, the specimens were subsequently rinsed multiple times with deionized water (Seralpur).

In situ microchemical analyses were carried out using a NewWave UP193 solid-state laser coupled to a Thermo-Finnigan Element2 HR-ICP-MS at the Department of Geosciences, University of Bremen. Isotope abundances of ^{25}Mg, ^{27}Al, ^{43}Ca, ^{55}Mn, ^{57}Fe and ^{87}Sr in foraminifera shells were determined at an irradiance of 1.3 GW cm^{-2}, a laser pulse rate of 5 Hz and a spot size of 50–100 µm. Plasma power was 1200 W, and Helium (0.7 L min^{-1}) and Argon (0.9 L min^{-1}) were used as sample and make-up gases, respectively. All isotopes were analysed at low resolution with five samples in a 20% mass window and a total dwell time of 25 ms per isotope. Blanks were measured for 30 s prior to ablation

and every analysis was followed by a wash out time of at least 60 s to avoid cross-contamination between samples.

A glass reference material (NIST610) was measured before every five ablation spots as an external
180 calibration standard using the values of Jochum et al. (2011). To assess data quality, a pressed pellet of MACS-3 carbonate standard powder (n=4) and the USGS reference material BHVO-2G (n=18) were analysed as control standards along with the samples. External precision is better than 3.9%, and accuracy as determined by comparison of our reference material data with the GeoReM database (as of July 2020) is better than 3.4% for all elements except for Mg (7.7%). The ^{43}Ca isotope was used
185 as an internal standard.

All shells were ablated from the outside to the inside. The number of shells analysed are provided in Table 1 and 2. In general, one profile was obtained for the three youngest chambers each. Data reduction followed an approach inspired by LAtools (Branson et al., 2019) and involved despiking of
190 the count sequences through removal of data points more than 4 times the interquartile range away from the 9 point moving median value. Subsequently, background values were removed and values below the limit of detection were omitted from the sequences prior to normalisation to 40% Ca and conversion to molar element/calcium ratios. Next to the first few seconds of each ablation profile that show anomalously high values, intervals where Mg/Ca correlated with either Al/Ca, Fe/Ca or
195 Mn/Ca were excluded from the calculations. All minor element/Ca profiles are made available in the supplementary information.
The presence of a low Mg/Ca layer at the outside of the shell wall, i.e. the presence of a crust, was assessed using a one-sided t-test. First, the highest and lowest points in a 11-point Gaussian smoothed profile were found and the 11 points on both sides of the maximum and minimum were
200 compared. Only profiles that showed a significantly (99% confidence interval) lower Mg/Ca layer at the outside of the test wall were considered to be encrusted. This chemistry based classification is consistent with visual observations on a selected number of shells and we therefore deem this classification not only reproducible, but also robust. Given long mixing times of our laser ablation system, the transition between crust and lamellar calcite cannot always be determined exactly. To
205 use an operationally easy and reproducible method, the length of the crust and the lamellar calcite parts within the profiles is therefore based on the number of data points below and above the value right between the crust and lamellar calcite Mg/Ca ratio.

The stable oxygen isotope data and the Mg/Ca data are compared to predicted values based on
210   climatology for the sediment data and on CTD measurements for the plankton tow data. Expected $\delta^{18}O$ equilibrium values are calculated using temperature and salinity from the World Ocean Atlas 1998 using the Shackleton (1974) palaeotemperature calibration and a regional $\delta^{18}O$ seawater-salinity relationship (LeGrande & Schmidt, 2006). Correction of the VSMOW to the VPDB scale was done by subtracting 0.20‰. For Mg/Ca we used a regional calibration specific for *G. inflata*
215   (Groeneveld & Chiessi, 2011).

Data processing and visualisation was done with R (R Core Team, 2019) using the packages openxlsx (Walker, 2019), zoo (Zeileis & Grothendieck, 2005), permute (Simpson, 2019), tidyverse (Wickham, 2017), egg (Auguie, 2019), ggpubr (Kassambara, 2019) and ggridges (Wilke, 2020).

Results

220

We first address the effect of cryptic diversity on *G. inflata* $\delta^{18}O$ and $\delta^{13}C$. In core GeoB13862-1 both genotypes of *G. inflata* are present at about equal abundances (SFig. 1). Non-encrusted specimens of genotype I were rare (< 3% on average) and no non-encrusted specimens of type II were found. We measured stable isotopes in 11 samples of non-encrusted genotype I and 30 each on encrusted
225   genotype I and II. Stable oxygen isotope ratios vary between 0.3 and 3.4 ‰, with non-encrusted specimens of genotype I having low values and encrusted specimens of both genotypes predominantly values above 2 ‰ (Fig. 4). The difference in $\delta^{18}O$ between encrusted and non-encrusted specimens of type I is about 2 ‰ in $\delta^{18}O$ and statistically significant (p = 2.70e-09; h_a: μ_{crust} > $\mu_{nocrust}$). We observe no statistically significant difference between encrusted specimens of
230   genotype I and II (p = 0.92; h_a: μ_{typeI} < μ_{typeII}). Stable carbon isotope ratios vary between 0.3 and 1.9 ‰ and show no effect of either crusting or genotypes (p = 0.95 (h_a: μ_{crust} ≠ $\mu_{nocrust}$) and 0.82 (h_a: μ_{typeI} ≠ μ_{typeII}) respectively). These results also hold when each interval for which at least 4 measurements are available is treated individually (supplementary information). So in the following we treat the samples from this core as a single group and because we did not identify a direct genotype effect on
235   the isotope ratios focus on the effect of crusting only.

Encrusted specimens of *G. inflata* appear smooth on the outside of the shell and no pores are visible, but they can be transparent (Fig. 3). Broken shells reveal the presence of large blocky crystals in the outer layer of the shell wall, where the pores are still visible (Fig. 3). The proportion of non-
240   encrusted specimens was low, especially in the cold Malvinas Current (Fig. 5). We performed

measurements on encrusted and non-encrusted as well as on randomly picked shells; sample numbers are given in Table 1. Stable oxygen isotope ratios from *G. inflata* in the sediment transect generally fall within the range of predicted $\delta^{18}O$ assuming that calcification occurs within the upper 700 m of the water column (Fig. 5). The apparent calcification depth (i.e. the depth where the difference between predicted and observed $\delta^{18}O$ is smallest) appears greater within the Brazil Current compared to within the Malvinas Current, but it is difficult to constrain within the BMCZ (Fig. 5).

Despite the limited number of observations of crust-free specimens especially in the southern cores, measurements on randomly selected specimens suggest that we do capture the stable isotope variability within each sample to a degree that we can draw robust conclusions (Fig. 5). The stable carbon isotope ratios reveal no influence of crusting at any location (*p* values between 0.29 and 0.96), but the stable oxygen isotopes show a complex pattern (Fig. 5). In the cores north and south of the BMCZ there is no consistent difference between encrusted and non-encrusted specimens. (*p* = 0.33 and 0.29 for GeoB6209-2, and GeoB2722-1, respectively). However, specimens from the cores within the BMCZ show an effect of encrustation, with encrusted specimens having more positive $\delta^{18}O$. The effect is clearest in GeoB13862-1 (see above), but higher $\delta^{18}O$ of encrusted specimens is also apparent in GeoB6311-2, even though the difference is not significant, likely because of the low numbers (*p* = 0.11; h_a: $\mu_{crust} > \mu_{nocrust}$).

The Mg/Ca data from shells from the core tops show variability that exceeds the predictions based on a Mg/Ca-temperature calibration for whole (groups of) shells (Fig. 6). Crust Mg/Ca ratios in particular are below values expected within the upper 700 m of the water column. Even though non-encrusted specimens were rare, the laser ablation profiles through the shell walls allow us to assess the effect of crusting by comparison of the low and high Mg/Ca layers in the shells. This shows that in stark contrast to the stable oxygen isotope ratios, which also to a first order reflect temperature, we observe a large difference (median: ~1–2 mmol/mol) between the crust and the lamellar calcite at every site, not just in the confluence zone (Fig. 6).

As in the sedimentary shells, shells from the plankton tows display Mg/Ca variability that far exceeds predictions (Fig. 7a). Despite the spread in the Mg/Ca data and the offsets from the prediction, the data highlight four important aspects: i) both the lamellar calcite and the crust Mg/Ca decrease with water depth (Fig. 7a); ii) encrusted specimens are present as shallow as 80–100 m (the shallowest depth interval where *G. inflata* was present in numbers large enough for analysis) and not just at great depths (Fig. 7b); iii) the absence of a clear pattern in the degree of encrustation with depth

275 (Fig. 7c); and iv) no consistent vertical pattern in the difference between the Mg/Ca ratio of the lamellar calcite and of the crust calcite (Fig. 7d).

Discussion

Cryptospecies

Our measurements of stable oxygen and carbon isotope ratios of encrusted *G. inflata* genotypes I
280 and II from core GeoB13862-1 within the BMCZ do not show a significant difference between the two genotypes (Fig. 4). We cannot be completely sure that within the confluence zone both genotypes calcify in identical conditions as they may have different depth habitats, seasonal occurrences or even calcify with a different offset from equilibrium. Nevertheless, the most parsimonious explanation for the absence of a difference between the two genotypes is that they
285 both calcify in the BMCZ and that genotypical variation in *G. inflata* leaves no imprint on their stable isotope signal.

The $\delta^{18}O$ values from the cores north and south of the BMCZ hint at a shallower apparent calcification depth (ACD) in the Malvinas Current, where only genotype II occurs (Morard et al., 2016). However, within the BMCZ where both genotypes are present (i.e. sites GeoB13862-1 and
290 GeoB6311-2) the ACD of both species is indistinguishable (Fig. 5). This indicates that differences in the ACD are adaptations to the local hydrography that are shared by the two genotypes, rather than genotype-specific responses. In order to improve palaeoceanographic reconstructions based on *G. inflata* shell composition it is thus necessary to better understand the ecology of the species as a whole in order to constrain the vertical and/or seasonal recording bias (Jonkers & Kučera, 2017).

Crusting

The appearance of the crust on *G. inflata* is smooth (Fig. 3) and hence markedly different from the crusts consisting of large blocky crystals found on other Globorotalids or Neogloboquadrinids (Hemleben et al., 1985; Jonkers et al., 2012). However, in cross section the crust appears to consist of blocky crystals, more reminiscent of real crusts, despite its association with gametogenesis (Fig.
300 3d) (Hemleben et al., 1985). Crust formation (in *G. inflata*) needs to be studied in the laboratory to elucidate the processes controlling its origin and composition, but our data challenge the traditional view that crust formation is triggered by temperature and occurs deeper (than lamellar calcite) in the water column.

305 Our results from plankton tows further substantiate other observations on the incidence of crusting in the water column (Rebotim et al., 2019); even though encrusted specimens are more common at greater depth, they are not restricted to great depths only (Fig. 7). The higher Mg/Ca ratios of specimens collected closer to the sea surface also indicates that the shallow encrusted specimens are unlikely to have been mixed upwards, but rather calcified at higher temperatures at the depths

310 where they were found. Moreover, crust Mg/Ca ratios are always lower than those of lamellar calcite, irrespective of water depth and hence temperature (Fig. 7). The increase in the proportion of encrusted shells with depth apparently supports the notion that crust formation occurs at a greater depth than lamellar calcite formation, but crucially, does not require vertical migration. If crust formation occurred during, or in response to, descent in the water column, it should lead to an

315 increasing proportion of crust of the shell wall with depth, and a constant lamellar calcite Mg/Ca ratio with depth associated with an increasing difference in the Mg/Ca ratio between the lamellar and the crust calcite. Our data however, show no such trends (Fig. 7) and the direct observations from the plankton thus challenge the idea that crust formation occurs at depth only and is driven by temperature change. Instead, they indicate that crust formation occurs i) at any depth and ii) at the

320 same depth as where the lamellar calcite is precipitated. Thus, even though we cannot completely rule out (an effect of) ontogenetic vertical migration, this indicates that vertical migration is not required to explain the presence of crusts in *G. inflata* and suggests that the difference between crust and lamellar calcite Mg/Ca ratio is not related to temperature. This interpretation is consistent with the large difference in Mg/Ca between the crust and lamellar calcite in shells from core

325 GeoB2722-1 from the Malvinas Current (Fig. 6), where the water column is close to isothermal, especially during the winter months when *G. inflata* is most abundant (Jonkers & Kučera, 2015). The consistently lower Mg/Ca ratio of the crust in the other sediment samples is therefore unlikely to reflect temperature differences in the water column. This implies that past water column profiles cannot be reconstructed from microanalysis of single shells. It also means that mixing shells with

330 different crust to lamellar calcite ratios (proportions) adds considerable non-temperature related noise to temperature reconstructions based on Mg/Ca ratios of *G. inflata*.

Somewhat counter-intuitively, the difference between the crust and the lamellar calcite may be because the Mg/Ca ratio of the lamellar calcite is too high, rather than that of the crust too low.

335 Studies using high-resolution micro-analytical techniques have shown that temperature-independent Mg/Ca banding in the lamellar calcite is absent from the crust calcite in *G. inflata* (Hathorne et al., 2009) as well as in other species (Fehrenbacher & Martin, 2010; Jonkers et al.,

2016). The presence of banding alone would therefore already raise the average Mg/Ca ratio of the lamellar calcite compared to the crust calcite, even if the entire shell formed at constant

340 temperatures. Our laser ablation system, however, cannot resolve such fine scale spatial variability because of the relatively long wash-out time of the ablation chamber. We nevertheless assume banding to be present and to be responsible for the higher Mg/Ca ratio of the lamellar calcite in *G. inflata* (Fig. 8).

345 This raises the question if the high Mg/Ca bands are the only reason why the lamellar calcite has on average higher Mg/Ca ratios than the crust, or if the low Mg/Ca bands also have higher Mg/Ca than the crust? It is important to distinguish between those two possibilities as the former does not require a different mechanism of trace element incorporation of the crust and the lamellar calcite and hence presents a simpler model of calcification. Our results cannot answer this question, but

350 inspection of high-resolution Mg/Ca maps of *G. inflata* from previous work seems to indicate that the crust Mg/Ca is indeed similarly low as that of the calcite between the high Mg/Ca bands in the lamellar calcite (Hathorne et al., 2009). Answering this question requires very high resolution analyses that are able to accurately distinguish between the micrometer-scale bands in the lamellar calcite without any mixing (either because of a large pixel size in the case of mapping techniques or

355 because of mixing of material in the ablation chamber). Nevertheless, close inspection of Mg/Ca maps of studies on other species (Neogloboquadrinids) also reveals that the crust Mg/Ca ratio is not (markedly) different from the low Mg/Ca bands in the lamellar calcite (Davis et al., 2017; Fehrenbacher & Martin, 2010; Jonkers et al., 2016). The evidence thus suggests that a higher Mg/Ca ratio of the lamellar calcite compared to the crust of *G. inflata*, and perhaps other species of

360 planktonic foraminifera, may simply be due to the presence of high Mg/Ca bands and not because of shallower calcification or a different trace element incorporation mechanism.

If the difference in the Mg/Ca ratio between the crust and lamellar calcite is not due to calcification at different depths in the water column, then what mechanism could be responsible for the variable

365 difference in $\delta^{18}O$ along the studied transect? We rule out dissolution since this process acts at the population level and affects the average stable isotope ratios of the sedimentary population through preferential dissolution of non-encrusted shells, but does not directly affect the $\delta^{18}O$ of individual shells (Erez, 1978; Lohmann, 1995; Mekik & Winkelstern, 2020). Dissolution would therefore reduce the proportion of non-encrusted shells in the sediment, but not directly alter their $\delta^{18}O$. The

370 presence of clear layering in the Mg/Ca profiles at all sites also indicates that dissolution has not removed the lamellar calcite in encrusted shells (Fig. 6). Secondary ion mass spectrometry has

provided direct evidence that (gametogenic) crusts in other species of planktonic foraminifera may have higher $\delta^{18}O$ than lamellar calcite (Kozdon et al., 2009; Wycech et al., 2018). However, it remains unsubstantiated if the higher crust $\delta^{18}O$ in these studies is due to temperature as these

375 observations were made on sedimentary material. If such a contrast between crust and lamellar calcite $\delta^{18}O$ is also present in *G. inflata*, it appears i) unrelated to temperature (because the Mg/Ca data show that crusts are not formed at different temperatures than the lamellar calcite) and ii) variable in space. Even though the number of observations is relatively low, the spatial variability in the crust effect is statistically significant and it is difficult to explain if the crust were always formed

380 deeper than the lamellar calcite. The variable effect may therefore be fortuitous and reflect mixing of populations with and without a crust grown under different circumstances. This could be due to growth at different depths, seasons or advective mixing of shells by ocean currents. The largest and clearest difference in $\delta^{18}O$ due to crusting is indeed observed in core GeoB13862-1 from within the highly dynamic Brazil-Malvinas Confluence Zone (Fig. 5). Non-encrusted specimens are rare to

385 absent in colder waters, which may be suggestive of a thermal influence on crust incidence, rather than crust formation and/or composition. It could also be due to preferential preservation of encrusted shells, but we note that encrusted shells of *G. inflata* are also more common at greater water depth in the plankton tows, which is consistent with a thermal influence on crust incidence. Notwithstanding, it renders the possibility of finding a spurious crust effect in an area where warm

390 and cold waters meet larger. This hypothesis is consistent with observations from the North Atlantic, where a difference between encrusted and non-encrusted $\delta^{18}O$ of *G. inflata* was observed near the Azores Front, but not along the Iberian Margin (Rebotim et al., 2019). It is also consistent with the absence of a crust effect on $\delta^{13}C$, even though $\delta^{13}C$ in planktonic foraminifera is more difficult to interpret (Jonkers et al., 2013; Spero et al., 1997) and we lack information on the shape of the

395 regional vertical profile of $\delta^{13}C$ of dissolved inorganic carbon.

Altogether, our data thus indicate that variability in $\delta^{18}O$ of the population of *G. inflata* at the BMCZ does not arise from genotypical variability, nor from vertical migration during ontogeny and crust formation at greater depth in the water column. The majority of the encrusted specimens in the

400 BMCZ have overlapping high $\delta^{18}O$ values, which means that encrusted type I and II co-occur in the BMCZ and predominantly calcify under the same conditions (Fig. 4). This is in agreement with their overlapping thermal niches (Morard et al., 2013). The variability in the $\delta^{18}O$ of *G. inflata* in the BMCZ is within the range of predicted $\delta^{18}O$ (Fig. 5), suggesting that differences between encrusted and non-encrusted (genotype I) specimens could be explained by local hydrographic variability alone.

405 However, further north, where vertical temperature gradients are at least as steep, we observe no

effect of encrustation (Fig. 5), suggesting that variability in δ^{18}O due to encrusting in *G. inflata* reflects horizontal or temporal (seasonal), rather than vertical, hydrographic variability.

A small part of the population of *G. inflata* in the BMCZ may therefore have grown during summer, or have been advected from the warmer Brazil Current. It should however be noted that advection

410 or growth during summer appears rare because non-encrusted specimens are rare (< 3%) and because encrusted genotype I specimens with a Brazil Current or summer signature make up only a small proportion of the population in the core in the confluence zone (29 out of 34 samples of encrusted genotype I have δ^{18}O values >2.5; Fig. 5). Nevertheless, mixing encrusted and non-encrusted specimens of *G. inflata* for stable isotope analysis may lead to spatially and temporally

415 variable bias, which should be considered when interpreting time series of δ^{18}O of this species. Since the proportion of the crust is variable among *G. inflata* shells, we recommend performing replicate analyses to assess the magnitude of this bias.

The potential of advection of the genotype I specimens from the warm Brazil Current into BMCZ,

420 could offer a possible mechanism for the generation of cryptic diversity in *G. inflata* if some specimens managed to cross the frontal zone. *Globorotalia inflata* initially appeared during the early Pliocene in the temperate Southwest Pacific (4.14 Ma; (Scott et al., 2007)) and invaded the transitional and subtropical waters of both hemispheres by 2.09 Ma (Berggren et al., 1995). Only around 700 ka did the species expand its geographical range into the southern subpolar waters

425 (Keany & Kennett, 1972; Kennett, 1970). This is the potential speciation event that may have led to the establishment of genotype II. Speciation in the open ocean is notoriously difficult due to the lack of physical barriers that interrupt gene flow between populations. However, frontal zones of the southern hemisphere may provide rare examples of such barriers, since it took *G. inflata* more than a million years to cross the subpolar front in the southern hemisphere. Occasional southward

430 crossing of the front by *G. inflata* may have allowed establishment of a pioneer population that eventually evolved into a separate genotype because a gene flux capable of keeping the genetic homogeneity between the two could not be maintained.

Conclusions

We analysed stable oxygen and carbon isotopes and Mg/Ca of *G. inflata* from sediment and water

435 column samples from the western South Atlantic to assess the effects of cryptospecies and encrustation on the environmental signal preserved in their shell composition.

We find no statistically significant difference in the δ¹⁸O and δ¹³C of encrusted warm and cold water genotypes of *G. inflata* measured on sedimentary samples from a core in the Brazil-Malvinas Confluence Zone. We hence conclude that besides differences in ecology, genotypical variability leaves no direct imprint on the species δ¹⁸O and δ¹³C values. This means that for the interpretation of stable isotope time series of this species cryptospecies effects can be ignored, but ecological preferences need to be considered.

Encrustation has a markedly variable effect on δ¹⁸O values. We find significant differences between encrusted and non-encrusted shells in the highly dynamic Brazil-Malvinas Confluence Zone, but little, if any differences in cores to the north and south of the BMCZ. This variable crust effect on δ¹⁸O is in stark contrast with Mg/Ca, where we find that crust Mg/Ca ratios are consistently lower than those of lamellar calcite at all locations. In addition, plankton tow data show that vertical migration is not required to explain the lower Mg/Ca ratio in the crust because we find encrusted specimens close to the sea surface. Instead we hypothesise that the difference in Mg/Ca between the crust is due to the presence of non-temperature related banding only in the lamellar calcite that raises its average Mg/Ca ratio. Crust formation and composition thus appear not related to vertical migration. However, the higher proportion of encrusted shells deeper in the water column and in colder waters suggests that temperature may have an influence on crust incidence, rather than on its composition or formation. In any case, this could explain the previously accepted idea that crust formation is associated with downward vertical migration during ontogeny.

If vertical migration is not required to explain the compositional differences between crust and lameller calcite, then the spatially variable effect on δ¹⁸O values may be due to advective mixing of shells grown under different conditions. Indeed, the largest and clearest effect of encrustation on δ¹⁸O is found in the Brazil-Malvina Confluence Zone where steep horizontal thermal gradients exist and not at locations with steep vertical temperature gradients. Proxy time series of mixed encrusted and non-encrusted *G. inflata* may therefore present an integrated signal of a variable amount of non-temperature related noise (Mg/Ca) and a possible signal of lateral advection or seasonality.

Data availability statement

The stable isotope data, genotype counts and laser ablation data will be made publicly available on pangaea.de upon acceptance of this manuscript. For review the data can be accessed at:

- Stable isotopes: https://cloud.marum.de/s/LPGiYagBGBFC3TA.
- Count data for genotypes: https://cloud.marum.de/s/FmszoJgBQpwnFXb.

- LA-ICP-MS: raw counts and processed profiles:
  https://cloud.marum.de/s/zZEpwCgSQLpLRXM. The files contain raw and despiked element
470 counts, calibration factors and calibrated element/calcium ratios.

The world ocean atlas data were obtained from
https://psl.noaa.gov/data/gridded/data.nodc.woa98.html and the CTD data used in figure 7 from
https://doi.pangaea.de/10.1594/PANGAEA.895565.

475 # Acknowledgments

Figures

Fig. 1: Locations of the sediment and plankton tow samples used here. Background colours indicate annual mean seawater temperature. Note that for clarity the locations of sediment core GeoB13862-1 and plankton tow MP13 are offset; the thin dotted lines point to their real location.
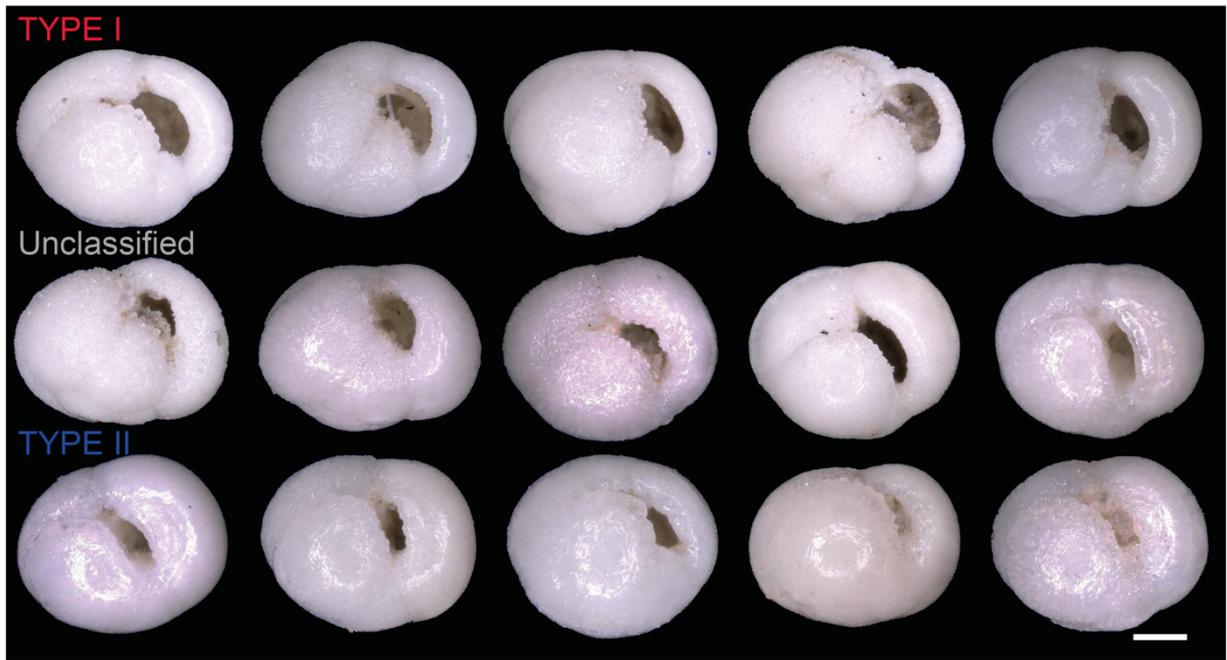
Fig. 2: Light microscopy images of examples specimens of *G. inflata* from the core GeoB13862-1. The specimens are classified in three categories based on the relative size of the aperture of the last chamber, with genotype I having a larger aperture than genotype II. Only the specimens with clear distinctive morphology are classified as either genotype I or II and the remaining specimens are group as intermediate and have not been used for geochemical analysis in this study. Scale bar 100 μm.

495

500
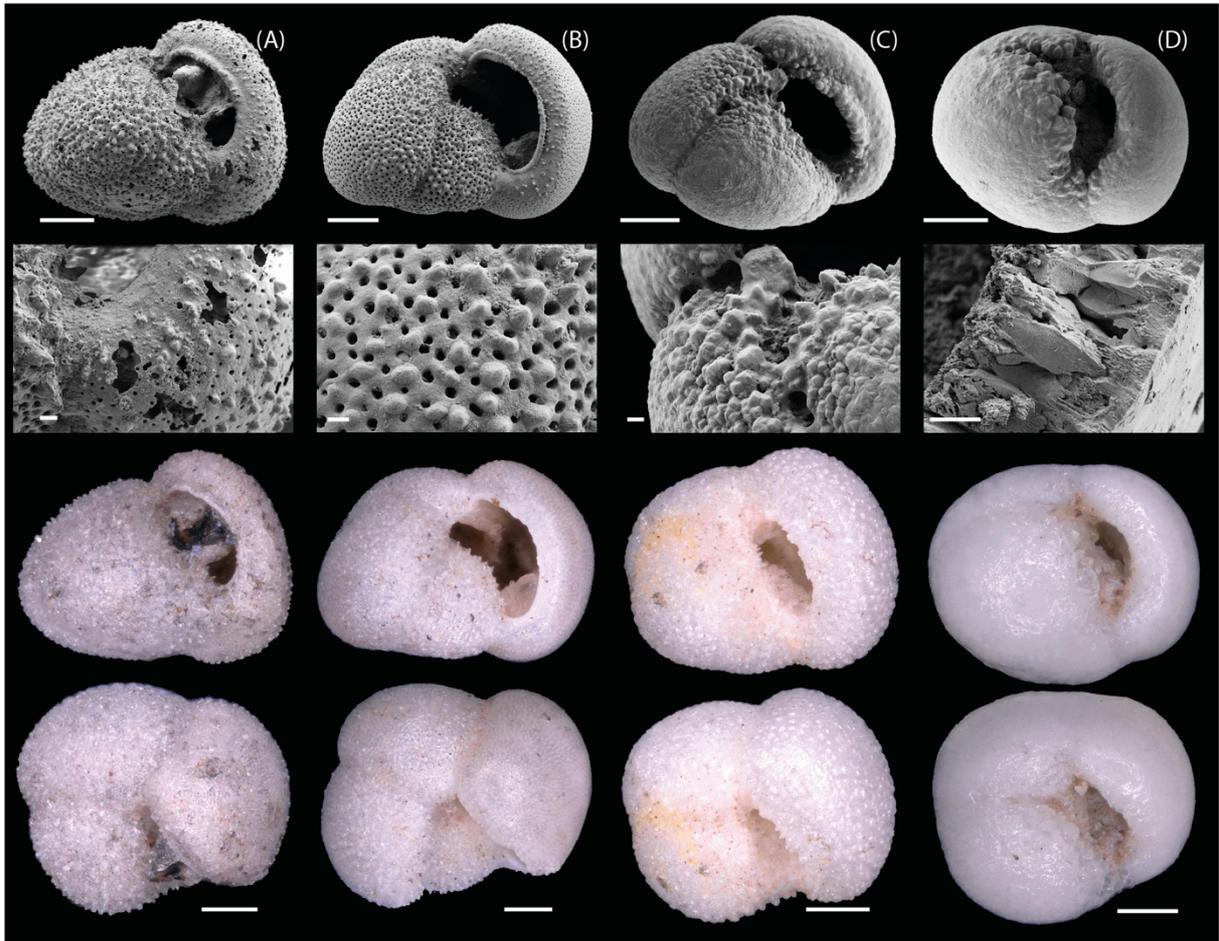
Fig. 3: SEM and light microscopy images illustrating the degrees of encrustation of *G. inflata*. (A) Crust free, (B) light, (C) medium and (D) full encrustation. The images represent the same specimens with SEM and light microscopy. The intensity of the encrustation is visible with the gradual smoothing of the surface of the shell. Scale bars are 100 μm for the full specimens for SEM and light microscopy and 10 μm for the details of the ultrastructure. Specimen A shows signs of dissolution and was not used for analysis.
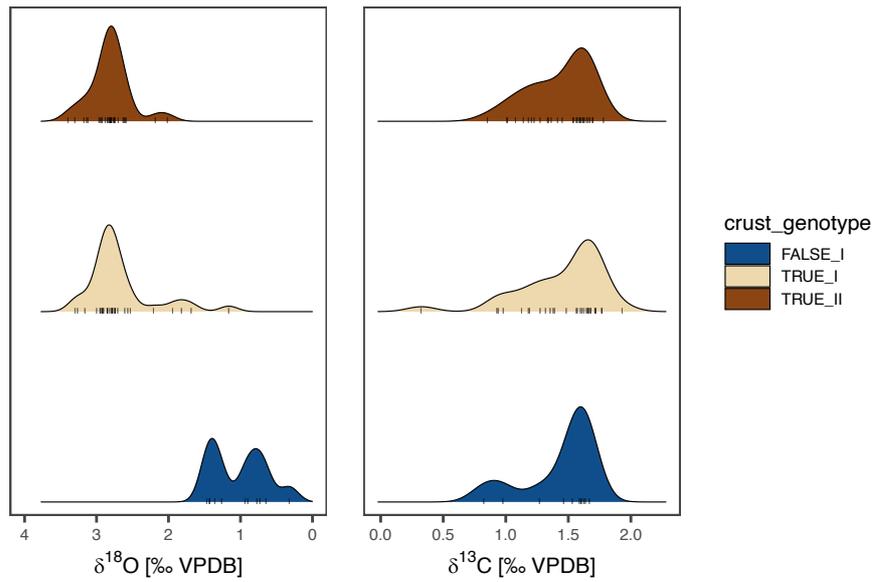
Fig. 4: Density plots of stable oxygen and carbon isotope ratios of *G. inflata* in core GeoB13862-1 from the Brazil-Malvinas Confluence Zone separated by genotype and crusting; note that non-encrusted genotype II were not found. Individual measurements are indicated with vertical bars. Encrusted genotypes I and II have indistinguishable $\delta^{18}O$ and $\delta^{13}C$, indicating that there is no direct cryptospecies effect on the stable isotope ratios of *G. inflata*. Encrusted specimens of genotype I have however significantly higher $\delta^{18}O$ than crust-free specimens from the same core.

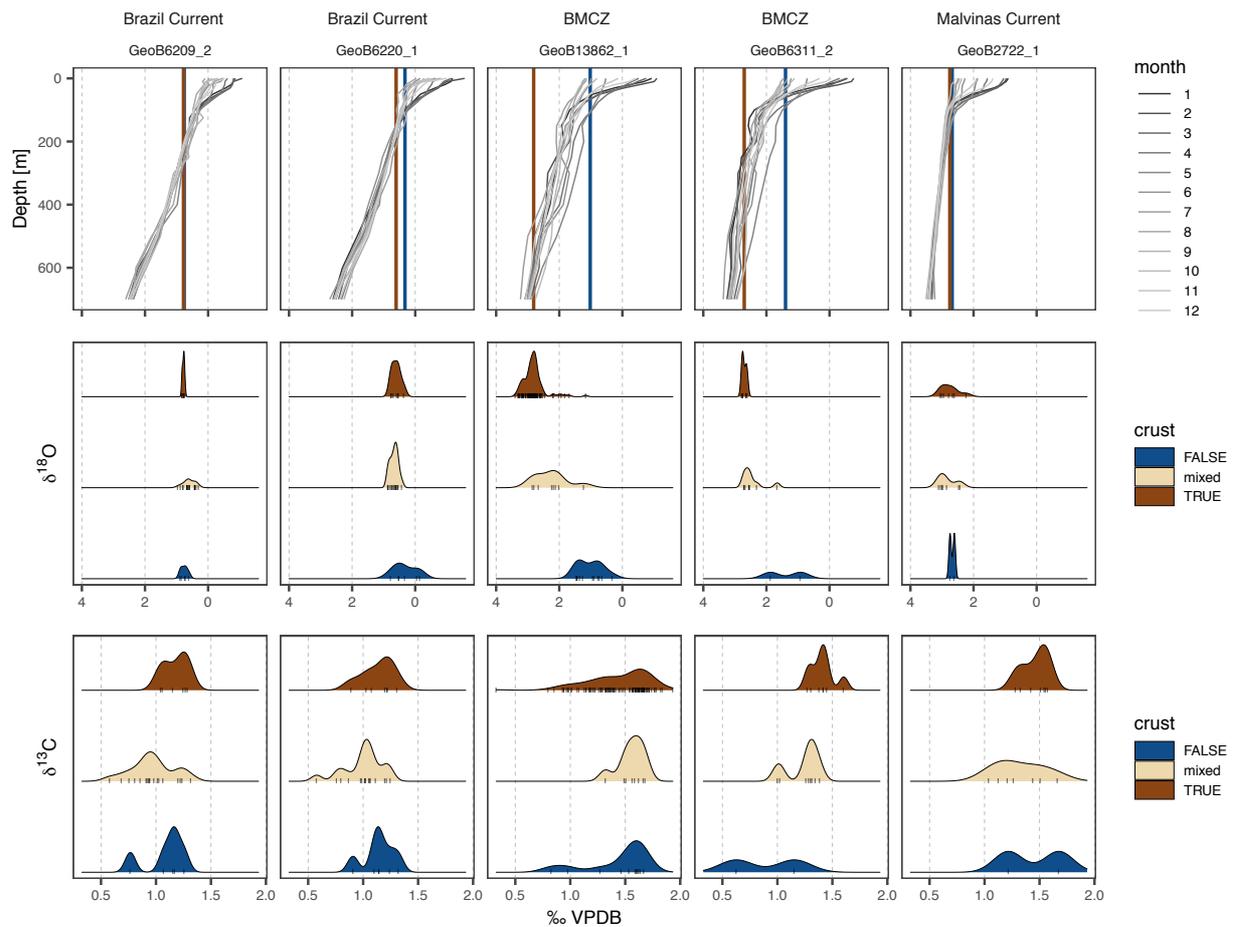Fig. 5: Sediment stable oxygen and carbon isotopes of *G. inflata*. The sites are ordered from north to south. Top row predicted δ¹⁸O for each site (see methods); coloured vertical bars indicate mean δ¹⁸O of crusted and non-encrusted shells. Middle and bottom rows show density plots of *G. inflata* δ¹⁸O and δ¹³C, respectively. Individual measurements are shown with thin vertical bars. The mean δ¹⁸O suggests a greater apparent calcification depth in the Brazil Current. The difference in δ¹⁸O between encrusted and non-encrusted *G. inflata* is clearest at the sites within the confluence zone and crusted and non-encrusted *G. inflata* have virtually indistinguishable δ¹⁸O in the Brazil Current, despite steep vertical gradients in δ¹⁸O. This indicates that the difference in δ¹⁸O between crusted and non-encrusted specimens is not associated with calcification of the lamellar calcite at shallower depth than the crust calcite and instead suggests that the crust effect is due to dynamic local hydrography.
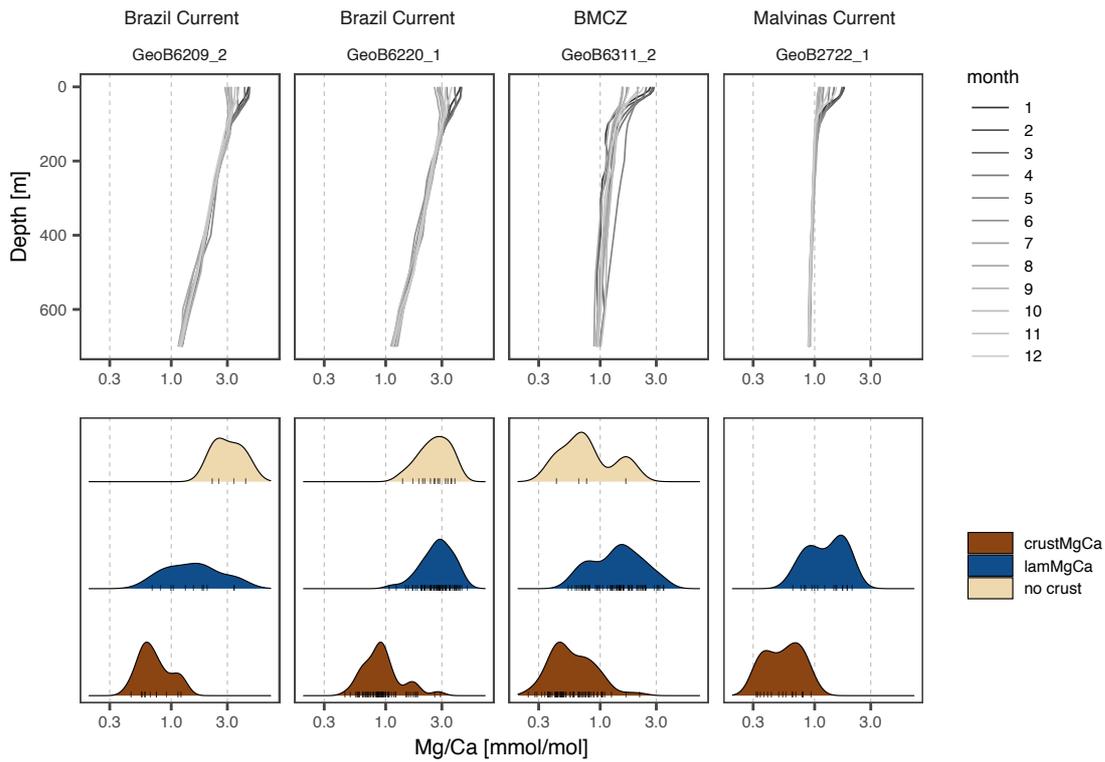
530

Fig. 6: Density plots of Mg/Ca ratios in profiles of *G. inflata* compared to predicted foraminifera
calcite Mg/Ca based on water temperature (methods). Sites are ordered from north to south and x
axes are on a logarithmic scale to reflect the non-linear temperature Mg/Ca relationship. Density
plot shows values for lamellar calcite and crust calcite for each profile (in general 3 per shell), where
535   a difference could be detected (see methods). Profiles where no crust could be detected are
indicated as no crust. In contrast to the stable oxygen isotopes the difference between crust and
lamellar calcite is observed at every site, even where the water column is almost isothermal (site
GeoB2722-1), suggesting that the difference between crust and lamellar calcite is not related to the
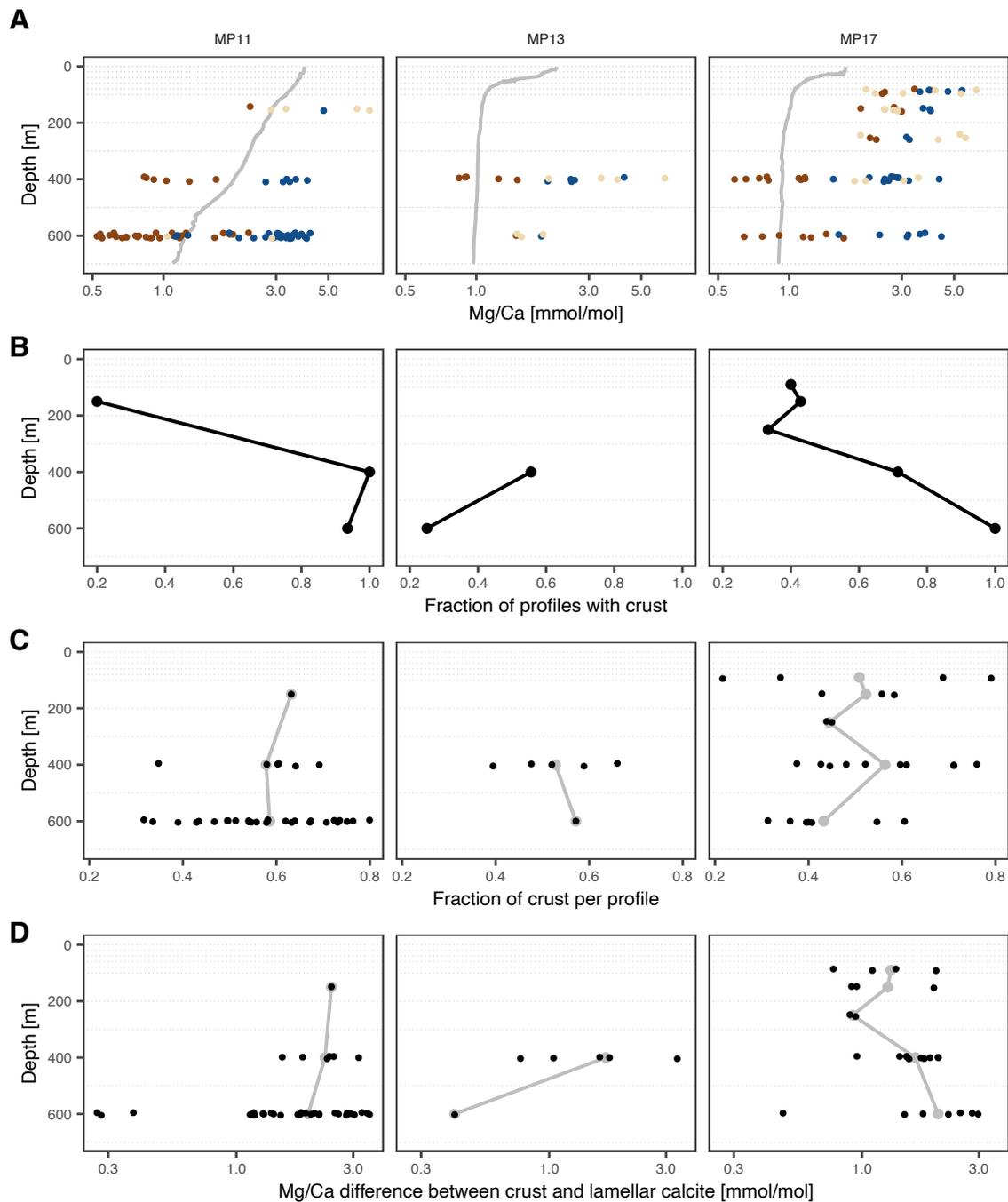vertical temperature gradient.

540

Fig. 7: Water column *G. inflata* Mg/Ca ratios and crust characteristics. Data from plankton tows; stations ordered from north to south; horizontal dotted lines indicate collection intervals. Vertical position of the points in A, C and D is jittered to enhance visibility. Note logarithmic x axis scale in top row. Grey lines in C and D connect the mean values for the collection intervals. A: Mg/Ca ratios of crust and lamellar calcite in profiles where layering could be detected (see methods, colours as in Fig. 6). The grey line is the predicted Mg/Ca ratio (see methods). B: General downward increase in the fraction of the shells (profiles) where a crust could be detected based on the Mg/Ca profile. C: No vertical trend in the fraction of crust per shell (profile). D: no vertical trend in the difference between crust and lamellar calcite. The presence of crusted shells at shallow depth together with

absence of clear trends in the thickness of the crust and the difference between the crust and the lamellar calcite indicate that crust formation is not associated with vertical ontogenetic migration.
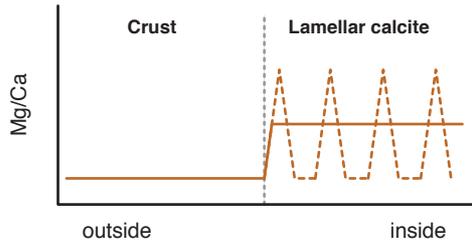
Fig. 8: Schematic Mg/Ca distribution through a *G. inflata* shell wall showing that the difference in the Mg/Ca ratio between the crust and the lamellar calcite reflects the presence of high Mg/Ca bands in the lamellar calcite that are unrelated to temperature. We infer that the crust Mg/Ca ratio is low simply because of the absence of banding and not necessarily because it formed deeper in the water column during downward ontogenetic migration. The dashed orange line reflects the real high-resolution Mg/Ca profile and the solid line the Mg/Ca profile measured using our laser ablation setup.

Tables

Table I: sediment sample details.

| Site	Device	Lat	Lon	Water depth (m)	Area	Stable isotope measurements (n samples)			LA-ICP-MS (n shells)
						Non-encrusted	Mixed	Encrusted	
GeoB6 209-2	multi-corer	-31.76	-48.15	3013	Brazil Current	5	18	6	5
GeoB6 220-1	multi-corer	-33.36	-49.39	2277	Brazil Current	6	16	7	27
GeoB1 3862-1	gravity corer	-38.02	-53.75	3588	BMCZ	11	8	96	NA
GeoB6 311-2	multi-corer	-38.81	-54.63	996	BMCZ	2	8	7	25
GeoB2 722-1	giant box corer	-47.33	-58.62	2355	Malvinas Current	2	7	7	5

Table II: stratified plankton net details.

Station	Lat	Lon	Date	LA-ICP-MS (n shells)
MP11 (M133-34-	-38.00	-53.42	2017-01-04	7

| 1)				
MP13 (M133-56-1)	-38.77	-53.97	2017-01-05	3
MP17 (M133-65-1)	-42.57	-57.99	2017-01-07	5

Supplementary information
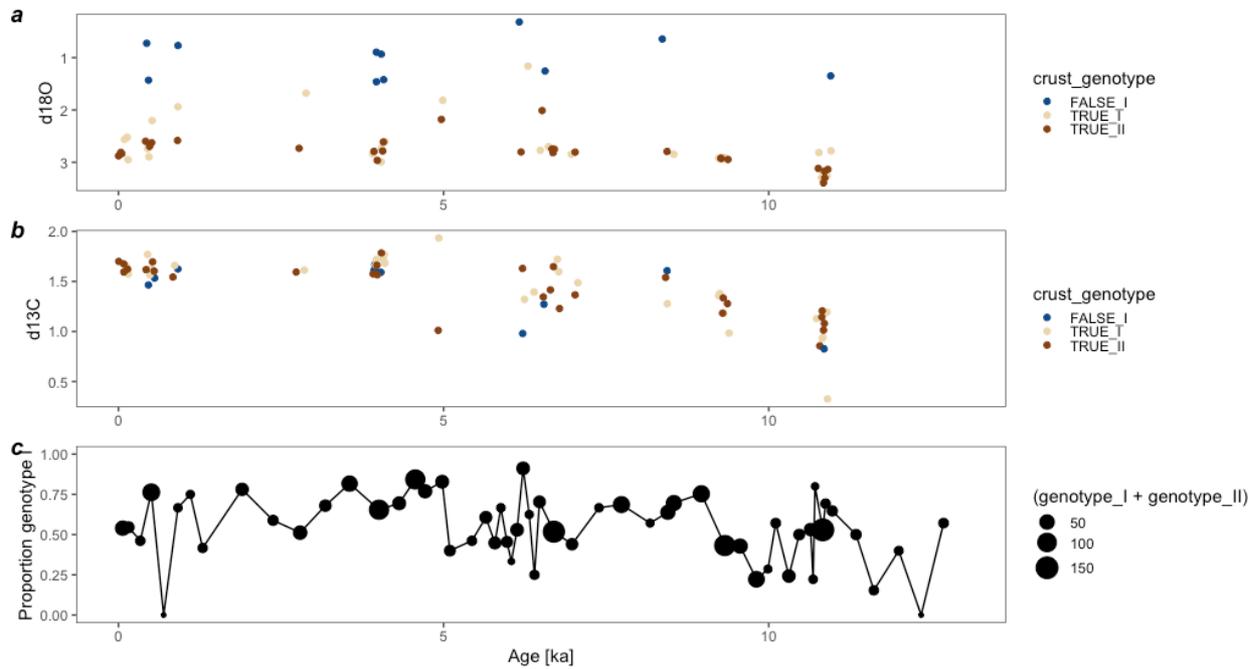
SFig. 1: downcore stable isotope data and genotype proportions in core GeoB13862-1 (ages from Vogt et al., 2015). The points in a and b have been slightly jittered in the x direction to improve clarity. Points in panel c are scaled to the number of *G. inflata* shells that could be assigned to the two genotypes.

There are three levels for which at least four samples of encrusted genotype I and II have been measured (7-9 cm, 258-260 cm and 875-877 cm; 0.07, 4.00 and 10.83 ka respectively). Paired t-tests reveal no difference in δ^{18}O or δ^{13}C between encrusted genotype I and II; p values for δ^{18}O: 0.84, 0.49 and 0.79; for δ^{13}C: 0.55, 0.30, 0.92.
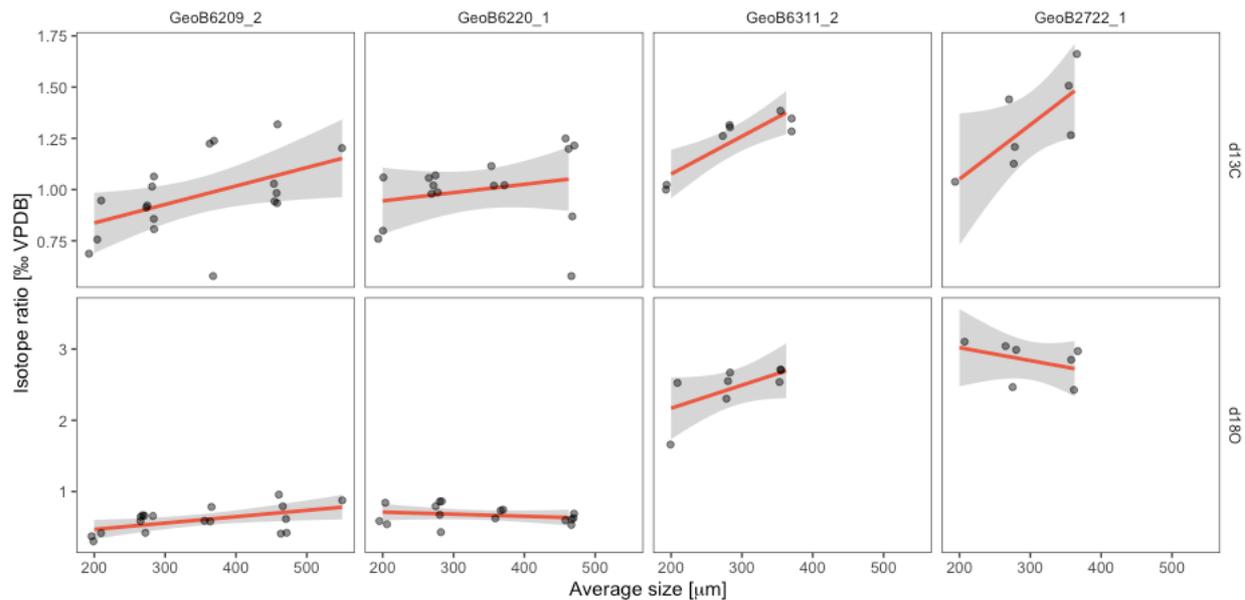
SFig 2: sieve size effect on stable isotope ratios of *G. inflata* in core top sediments. Data plotted at midpoint of size range and jittered slightly to improve visibility. Red lines show linear regression with 95 % confidence intervals in grey.

Note absence of consistent size effect on $\delta^{18}O$ which allows us to mix measurements on all size fractions and compare to the measurements in the 300–1000 µm fraction in core GeoB13862-1. There is a more consistent size effect on $\delta^{13}C$, with bigger shells having higher values. Genotype I is in general larger than genotype II; a potential difference in $\delta^{13}C$ would therefore be enhanced by the size effect. This implies that the similarity in $\delta^{13}C$ of the two genotypes in core GeoB13862-1 is most likely real and that there is therefore no genotype effect on the stable isotope ratios of *G. inflata*.

Element/calcium profiles can be viewed at https://cloud.marum.de/s/TC8dPL4eowknrEm and will be made available at Zenodo after acceptance of this manuscript. The grey rectangles indicate the filtered section used in the analyses.

References

Auguie, B. (2019). egg: Extensions for "ggplot2": Custom Geom, Custom Themes, Plot Alignment,
Labelled Panels, Symmetric Scales, and Fixed Panel Size (Version 0.4.5). Retrieved from
https://CRAN.R-project.org/package=egg

Bé, A. W. (1980). Gametogenic calcification in a spinose planktonic foraminifer, *Globigerinoides
sacculifer* (Brady). *Marine Micropaleontology*, *5*, 283–310. https://doi.org/10.1016/0377-
8398(80)90014-6

Bé, A. W., & Ericson, D. B. (1963). Aspects of calcification in planktonic Foraminifera (Sarcodina).
Annals of the New York Academy of Sciences, *109*, 65–81. https://doi.org/10.1111/j.1749-
6632.1963.tb13462.x

Bé, A. W., & Hutson, W. H. (1977). Ecology of Planktonic Foraminifera and Biogeographic Patterns of
Life and Fossil Assemblages in the Indian Ocean. *Micropaleontology*.
https://doi.org/10.2307/1485406

Berggren, W. A., Kent, D. V., Swisher, C. C., & Aubry, M.-P. (1995). A REVISED CENOZOIC
GEOCHRONOLOGY AND CHRONOSTRATIGRAPHY. *Geochronology, Time Scales, and Global
Stratigraphic Correlation*. https://doi.org/10.2110/pec.95.04.0129

Bolton, A., & Marr, J. P. (2013). Trace element variability in crust-bearing and non crust-bearing
Neogloboquadrina incompta, P–D intergrade and *Globoconella inflata* from the Southwest
Pacific Ocean: Potential paleoceanographic implications. *Marine Micropaleontology*.
https://doi.org/10.1016/j.marmicro.2013.03.008

Branson, O., Fehrenbacher, J. S., Vetter, L., Sadekov, A. Y., Eggins, S. M., & Spero, H. J. (2019).
LAtools: A data analysis package for the reproducible reduction of LA-ICPMS data. *Chemical
Geology*. https://doi.org/10.1016/j.chemgeo.2018.10.029

Davis, C. V., Fehrenbacher, J. S., Hill, T. M., Russell, A. D., & Spero, H. J. (2017). Relationships
Between Temperature, pH, and Crusting on Mg/Ca Ratios in Laboratory-Grown
Neogloboquadrina Foraminifera. *Paleoceanography*, *32*(11), 1137–1152.
https://doi.org/10.1002/2017PA003111

Eggins, S., Sadekov, A., & Dedeckker, P. (2004). Modulation and daily banding of Mg/Ca in tests by
symbiont photosynthesis and respiration: a complication for seawater thermometry? *Earth and
Planetary Science Letters*, *225*(3-4), 411–419. https://doi.org/10.1016/j.epsl.2004.06.019

Erez, J. (1978). *The Influence of differential production and dissolution on the stable isotope
composition of planktonic foraminifera*. Woods Hole, MA: Massachusetts Institute of
Technology and Woods Hole Oceanographic Institution. https://doi.org/10.1575/1912/1614

Fehrenbacher, J., & Martin, P. (2010). Mg/Ca variability of the planktonic foraminifera *G. ruber* s.s. and *N. dutertrei* from shallow and deep cores determined by electron microprobe image mapping. *IOP Conference Series: Earth and Environmental Science*, *9*, 012018. https://doi.org/10.1088/1755-1315/9/1/012018

635   Groeneveld, J., & Chiessi, C. M. (2011). Mg/Ca of *Globorotalia inflata* as a recorder of permanent thermocline temperatures in the South Atlantic. *Paleoceanography*. https://doi.org/10.1029/2010pa001940

Hathorne, E. C., James, R. H., & Lampitt, R. S. (2009). Environmental versus biomineralization controls on the intratest variation in the trace element composition of the planktonic

640   foraminifera *G. inflata* and *G. scitula*. *Paleoceanography*, *24*(4), 959. https://doi.org/10.1029/2009PA001742

Hemleben, C., Spindler, M., Breitinger, I., & Deuser, W. G. (1985). Field and laboratory studies on the ontogeny and ecology of some globorotaliid species from the Sargasso Sea off Bermuda. *Journal of Foraminiferal Research*, *15*(4), 254–272. https://doi.org/10.2113/gsjfr.15.4.254

645   Jochum, K. P., Weis, U., Stoll, B., Kuzmin, D., Yang, Q., Raczek, I., et al. (2011). Determination of Reference Values for NIST SRM 610-617 Glasses Following ISO Guidelines. *Geostandards and Geoanalytical Research*, *35*(4), 397–429. https://doi.org/10.1111/j.1751-908X.2011.00120.x

Jonkers, L., & Kučera, M. (2015). Global analysis of seasonality in the shell flux of extant planktonic Foraminifera. *Biogeosciences*. https://doi.org/10.5194/bg-12-2207-2015

650   Jonkers, L., & Kučera, M. (2017). Quantifying the effect of seasonal and vertical habitat tracking on planktonic foraminifera proxies. *Climate of the Past*. https://doi.org/10.5194/cp-13-573-2017

Jonkers, L., de Nooijer, L. J., Reichart, G.-J., Zahn, R., & Brummer, G.-J. A. (2012). Encrustation and trace element composition of *Neogloboquadrina dutertrei* assessed from single chamber analyses – implications for paleotemperature estimates. *Biogeosciences*.

655   https://doi.org/10.5194/bg-9-4851-2012

Jonkers, L., van Heuven, S., Zahn, R., & Peeters, F. J. C. (2013). Seasonal patterns of shell flux, δ^{18}O and δ^{13}C of small and large *N . pachyderma* (s) and *G . bulloides* in the subpolar North Atlantic. *Paleoceanography*, *28*(1), 164–174. https://doi.org/10.1002/palo.20018

Jonkers, L., Buse, B., Brummer, G.-J. A., & Hall, I. R. (2016). Chamber formation leads to Mg/Ca

660   banding in the planktonic foraminifer *Neogloboquadrina pachyderma*. *Earth and Planetary Science Letters*. https://doi.org/10.1016/j.epsl.2016.07.030

Kassambara, A. (2019). ggpubr: "ggplot2" Based Publication Ready Plots (Version 0.2.3). Retrieved from https://CRAN.R-project.org/package=ggpubr

Keany, J., & Kennett, J. P. (1972). Pliocene-early Pleistocene paleoclimatic history recorded in

665   Antarctic-Subantarctic deep-sea cores. *Deep Sea Research and Oceanographic Abstracts*.
       https://doi.org/10.1016/0011-7471(72)90038-1

Kennett, J. P. (1970). Pleistocene paleoclimates and foraminiferal biostratigraphy in subantarctic
       deep-sea cores. *Deep Sea Research and Oceanographic Abstracts*.
       https://doi.org/10.1016/0011-7471(70)90092-6

670   Kozdon, R., Ushikubo, T., Kita, N. T., Spicuzza, M., & Valley, J. W. (2009). Intratest oxygen isotope
       variability in the planktonic foraminifer *N. pachyderma*: Real vs. apparent vital effects by ion
       microprobe. *Chemical Geology*. https://doi.org/10.1016/j.chemgeo.2008.10.032

LeGrande, A. N., & Schmidt, G. A. (2006). Global gridded data set of the oxygen isotopic composition
       in seawater. *Geophysical Research Letters*, *33*(12), 15833.

675   https://doi.org/10.1029/2006GL026011

Lohmann, G. P. (1995). A model for variation in the chemistry of planktonic foraminifera due to
       secondary calcification and selective dissolution. *Paleoceanography*, *10*(3), 445–457.
       https://doi.org/10.1029/95PA00059

Lončarić, N., Peeters, F. J. C., Kroon, D., & Brummer, G.-J. A. (2006). Oxygen isotope ecology of
680   recent planktic foraminifera at the central Walvis Ridge (SE Atlantic). *Paleoceanography*.
       https://doi.org/10.1029/2005pa001207

Marshall, B. J., Thunell, R. C., Spero, H. J., Henehan, M. J., Lorenzoni, L., & Astor, Y. (2015).
       Morphometric and stable isotopic differentiation of Orbulina universa morphotypes from the
       Cariaco Basin, Venezuela. *Marine Micropaleontology*, *120*, 46–64.

685   https://doi.org/10.1016/j.marmicro.2015.08.001

Mekik, F., & Winkelstern, I. (2020). Field Testing the Fidelity of $\delta^{18}O$ and $\delta^{13}C$ in Reconstructing
       Upper Ocean Hydrography. *Paleoceanography and Paleoclimatology*, *35*(3), 1524.
       https://doi.org/10.1029/2020PA003880

Moffa-Sánchez, P., Born, A., Hall, I. R., Thornalley, D. J. R., & Barker, S. (2014). Solar forcing of North
690   Atlantic surface temperature and salinity over the past millennium. *Nature Geoscience*.
       https://doi.org/10.1038/ngeo2094

Morard, R., Quillévéré, F., Douady, C. J., de Vargas, C., de Garidel-Thoron, T., & Escarguel, G. (2011).
       Worldwide genotyping in the planktonic foraminifer *Globoconella inflata*: implications for life
       history and paleoceanography. *PloS One*, *6*(10), e26665.

695   https://doi.org/10.1371/journal.pone.0026665

Morard, R., Quillévéré, F., Escarguel, G., de Garidel-Thoron, T., de Vargas, C., & Kucera, M. (2013).
       Ecological modeling of the temperature dependence of cryptic species of planktonic
       Foraminifera in the Southern Hemisphere. *Palaeogeography, Palaeoclimatology,*

Palaeoecology, *391*, 13–33. https://doi.org/10.1016/j.palaeo.2013.05.011

700   Morard, R., Reinelt, M., Chiessi, C. M., Groeneveld, J., & Kucera, M. (2016). Tracing shifts of oceanic
fronts using the cryptic diversity of the planktonic foraminifera *Globorotalia inflata*.
Paleoceanography, *31*(9), 1193–1205. https://doi.org/10.1002/2016PA002977

Mortyn, P. G., & Charles, C. D. (2003). Planktonic foraminiferal depth habitat and δ 18 O calibrations:
Plankton tow results from the Atlantic sector of the Southern Ocean : SURFACE STRATIFICATION

705   AND δ 18 O CALIBRATIONS. *Paleoceanography*, *18*(2). https://doi.org/10.1029/2001PA000637

Niebler, H.-S., & Gersonde, R. (1998). A planktic foraminiferal transfer function for the southern
South Atlantic Ocean. *Marine Micropaleontology*, *34*(3-4), 213–234.
https://doi.org/10.1016/S0377-8398(98)00009-7

Orr, W. N. (1967). Secondary calcification in the foraminiferal genus globorotalia. *Science*, *157*(3796),

710   1554–1555. https://doi.org/10.1126/science.157.3796.1554

van Raden, U. J., Groeneveld, J., Raitzsch, M., & Kucera, M. (2011). Mg/Ca in the planktonic
foraminifera *Globorotalia inflata* and *Globigerinoides bulloides* from Western Mediterranean
plankton tow and core top samples. *Marine Micropaleontology*.
https://doi.org/10.1016/j.marmicro.2010.11.002

715   R Core Team. (2019). R: A language and environment for statistical computing (Version 3.6.2). R
Foundation for Statistical Computing, Vienna, Austria. Retrieved from https://www.R-
project.org/

Rebotim, A., Voelker, A. H. L., Jonkers, L., Waniek, J. J., Schulz, M., & Kucera, M. (2019). Calcification
depth of deep-dwelling planktonic foraminifera from the eastern North Atlantic constrained by

720   stable oxygen isotope ratios of shells from stratified plankton tows. *Journal of
Micropalaeontology*. https://doi.org/10.5194/jm-38-113-2019

Sadekov, A. Y., Darling, K. F., Ishimura, T., Wade, C. M., Kimoto, K., Singh, A. D., et al. (2016).
Geochemical imprints of genotypic variants of *Globigerina bulloides* in the Arabian Sea.
Paleoceanography. https://doi.org/10.1002/2016pa002947

725   Santos, T. P., Ballalai, J. M., Franco, D. R., Oliveira, R. R., Lessa, D. O., Venancio, I. M., et al. (2020).
Asymmetric response of the subtropical western South Atlantic thermocline to the Dansgaard-
Oeschger events of Marine Isotope Stages 5 and 3. *Quaternary Science Reviews*, *237*, 106307.
https://doi.org/10.1016/j.quascirev.2020.106307

Scott, G. H., Kennett, J. P., Wilson, K. J., & Hayward, B. W. (2007). Globorotalia puncticulata:

730   Population divergence, dispersal and extinction related to Pliocene–Quaternary water masses.
Marine Micropaleontology. https://doi.org/10.1016/j.marmicro.2006.08.007

Shackleton, N. J. (1974). Attainment of isotopic equilibrium between ocean water and the benthonic

foraminifera genus uvigerina: Isotopic changes in the ocean during the last glacial. *Colloques Internationaux. Centre National de La Recherche Scientifique* , *219*, 203–209.

735   Simpson, G. L. (2019). permute: Functions for Generating Restricted Permutations of Data (Version 0.9-5). Retrieved from https://CRAN.R-project.org/package=permute

Spero, H. J., Bijma, J., Lea, D. W., & Bemis, B. E. (1997). Effect of seawater carbonate concentration on foraminiferal carbon and oxygen isotopes. *Nature*, *390*(6659), 497–500. https://doi.org/10.1038/37333

740   Spero, H. J., Eggins, S. M., Russell, A. D., Vetter, L., Kilburn, M. R., & Hönisch, B. (2015). Timing and mechanism for intratest Mg/Ca variability in a living planktic foraminifer. *Earth and Planetary Science Letters*, *409*, 32–42. https://doi.org/10.1016/j.epsl.2014.10.030

Walker, A. (2019). openxlsx: Read, Write and Edit XLSX Files (Version 4.1.0.1). Retrieved from https://CRAN.R-project.org/package=openxlsx

745   Wickham, H. (2017). *tidyverse: Easily Install and Load the "Tidyverse"* [1.2.1]. Retrieved from https://CRAN.R-project.org/package=tidyverse

Wilke, C. O. (2020). ggridges: Ridgeline Plots in "ggplot2" (Version 0.5.2). Retrieved from https://CRAN.R-project.org/package=ggridges

Wilke, I., Bickert, T., & Peeters, F. J. C. (2006). The influence of seawater carbonate ion concentration

750   [CO32−] on the stable carbon isotope composition of the planktic foraminifera species Globorotalia inflata. *Marine Micropaleontology*, *58*(4), 243–258. https://doi.org/10.1016/j.marmicro.2005.11.005

Wycech, J. B., Kelly, D. C., Kitajima, K., Kozdon, R., Orland, I. J., & Valley, J. W. (2018). Combined Effects of Gametogenic Calcification and Dissolution on δ^{18}O Measurements of the Planktic

755   Foraminifer *Trilobatus sacculifer*. *Geochemistry, Geophysics, Geosystems*, *19*(11), 4487–4501. https://doi.org/10.1029/2018GC007908

Zeileis, A., & Grothendieck, G. (2005). zoo : S3 Infrastructure for Regular and Irregular Time Series. *Journal of Statistical Software*, *14*(6). https://doi.org/10.18637/jss.v014.i06